NANO LETTERS

LETTER

pubs.acs.org/NanoLett

Multiple-Wavelength Focusing of Surface Plasmons with a Nonperiodic Nanoslit Coupler

Takuo Tanemura,[*,†,‡] Krishna C. Balram,[†] Dany-Sebastien Ly-Gagnon,[†] Pierre Wahl,[†,§] Justin S. White,[∥] Mark L. Brongersma,[∥] and David A. B. Miller[†]

[†]Edward L. Ginzton Laboratory, Stanford University, Stanford California 94305-4088, United States

[‡]Research Center for Advanced Science and Technology, University of Tokyo, Tokyo 153-8904, Japan

[§]Brussels Photonics Team, Applied Physics and Photonics Department, Pleinlaan 2, Vrije Universiteit Brussel, Brussels 1050, Belgium

[∥]Geballe Laboratory for Advanced Materials, Stanford University, Stanford, California 94305, United States

Supporting Information

ABSTRACT: A novel type of multiple-wavelength focusing plasmonic coupler based on a nonperiodic nanoslit array is designed and experimentally demonstrated. An array of nanoslits patterned on a thin metal film is used to couple free-space light into surface plasmon polaritons (SPPs) and simultaneously focus different-wavelength SPPs into arbitrary predefined locations in the two-dimensional plane. We design and fabricate a compact triplexer on a glass substrate with an integrated silicon photodetector. The photocurrent spectra demonstrate that the incident light is effectively coupled to SPPs and routed into three different focal spots depending on the wavelength. The proposed scheme provides a simple method of building wavelength-division multiplexing and spectral filtering elements, integrated with other plasmonic and optoelectronic devices.

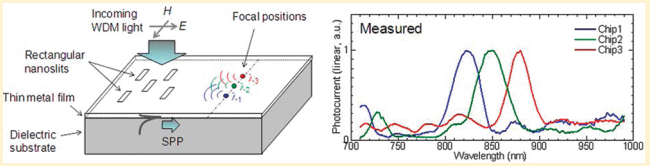

KEYWORDS: Surface plasmon polariton, wavelength demuliplexer, optical interconnects, spectral imaging

Surface plasmon polaritons (SPPs), described as surface electromagnetic waves coupled to collective oscillations of free electrons in a metal, have generated substantial interest in the diverse fields of biosensing, nonlinear optics, photovoltaics, and integrated nanophotonic devices.[1−4] Owing to the strong confinement of light at the metal−dielectric interface, SPPs offer a unique two-dimensional (2D) optical platform to manipulate light at a subwavelength scale. A series of SPP-based nanophotonic components have been demonstrated, including SPP launchers, lenses, guides, mirrors, beam splitters, and interferometers.[1,4−10] Another potentially useful component would be a compact plasmonic wavelength demultiplexer that could focus SPPs at different wavelengths to individual waveguides or photodetecting elements. Such a device would be extremely important for the wavelength-division-multiplexed (WDM) optical interconnects, as well as spectral imaging and sensing applications. Several schemes of SPP demultiplexers have been demonstrated to date, including those employing bull's-eye antennas,[11] plasmonic crystals,[12] and concentric groove gratings.[13] While most of these previous works were based on essentially periodic structures, such as gratings or crystals, it has been realized that the use of nonperiodic structures may both lead to higher performance and novel kinds of device function beyond those available in periodic structures. For example, nonperiodic dielectric stacks can substantially outperform periodic ones for superprism wavelength splitting and allow novel functionalities such as steplike wavelength dispersion.[14] A nonperiodic structure has also been applied recently to binary-patterned plasmonic couplers to demonstrate multiple-spot focusing functions, which are not readily possible using periodic grating couplers.[15] In this work, we extend the nonperiodic approaches to nanometallic wavelength-splitting devices and demonstrate a novel nanoslit array structure, which allows simultaneous coupling and focusing of multiple-wavelength SPPs into different positions in the 2D plane of the metal−dielectric interface. As a proof-of-concept, a triplexer is designed using an iterative optimization algorithm and fabricated on a glass substrate with an integrated silicon photodetector. The photocurrent spectra demonstrate that the incident light is effectively coupled to SPPs and routed to three different focal positions depending on its wavelength.

A schematic of the proposed wavelength-demultiplexing SPP coupler is shown in Figure 1. A nonperiodic array of rectangular nanoslits is formed through the metal film. Each slit is subwavelength in size in the *x* direction and is roughly half a wavelength in the *y* direction, so that it supports a single waveguide mode inside the slit. When an *x*-polarized light beam (electric field polarized in *x*-direction) is shone perpendicularly to the surface onto the metal film, each slit acts as a point dipole source of SPPs that propagates in the plane of the metal film at the bottom metal-dielectric interface. With relatively thin metal and narrow slits as employed in this work, we can neglect the effect of multiple reflections or scatterings among different slits, and simply apply the Huygens−Fresnel principle; the waves generated at multiple nanoslits add up coherently in the 2D plane.[8,16] By carefully

Received: March 21, 2011
Revised: May 23, 2011
Published: May 31, 2011

choosing the location of each slit using an iterative algorithm discussed below, the wavefront of SPPs could be controlled to obtain simultaneous focusing of multiple different wavelengths to different spots at the edge of the metal film.

To describe the design approach, let us consider that N slits are located at the positions $\mathbf{r}_n^S$ ($n = 1, ..., N$) on the 2D plane of a metal film and that we want to focus waves at M different wavelengths λ_m to individual locations $\mathbf{r}_m^F$ ($m = 1, ..., M$) on the film (in our example below, these locations are chosen to be at the edge of the film). In the regime where $|\mathbf{r}_m^F - \mathbf{r}_n^S|$ is larger than several SPP wavelengths, the electric field of the SPP wave radiated from a point dipole source in the 2D plane can be well approximated to have a $\cos\theta_{n,m}/|\mathbf{r}_m^F - \mathbf{r}_n^S|$ dependence, where $\theta_{n,m}$ is the angle between the x axis and the vector $\mathbf{r}_m^F - \mathbf{r}_n^S$ as defined in Figure 2a.[16] The complex amplitude of the electric field at the focus position m is then written as

$$E_m^{\text{total}} = \sum_n E_{n,m} \qquad (1)$$

where $E_{n,m}$ describes the contribution from slit n to focus m, which can be calculated approximately[16] using the expression

$$E_{n,m} = A_{n,m} T_{n,m} \frac{\cos\theta_{n,m}}{\sqrt{|\mathbf{r}_m^F - \mathbf{r}_n^S|}} \exp[ik_m^{\text{SPP}}(\mathbf{r}_m^F - \mathbf{r}_n^S)] \qquad (2)$$

Here, k_m^{SPP} is the propagation constant of the SPP wave, $A_{n,m}$ is the excited field amplitude at slit n, and $T_{n,m}$ is the complex transmission coefficient, which accounts for the total scattering loss and phase shift that the SPP experiences by crossing over other slits. Note that all of these parameters have index m since they depend on the focusing wavelength λ_m. To derive $A_{n,m}$ and $T_{n,m}$, we numerically calculate the wavelength dependence of SPP excitation efficiency and transmission by finite-difference-time-domain (FDTD) simulation. For simplicity, in deriving $T_{n,m}$, we assume $T_{n,m} = t_m^{p_n}$, where t_m is the transmission over a single slit at a normal angle and p_n is the number of slits to cross. In our example below, p_n was approximated simply by the number of slit columns located between the slit n and the right metal edge where the foci are located. Despite these rather radical approximations, we find that the optimization results do not depend significantly on the accuracy of $T_{n,m}$; for the slit geometry used in our work, this is because SPPs scatter relatively weakly (and more importantly suffer little optical phase shift) as they interact with other slits in the structure.

The nonperiodic slit structure is designed using an iterative method. The optimization algorithm closely follows the method previously proposed for designing a dielectric holographic grating coupler.[17] The flowchart of the algorithm is described in Figure 2c. In each iteration step, we first calculate the total electric field E_m^{total} at the corresponding wavelength λ_m for each of the respective focus positions ($m = 1, ..., M$) using eqs 1 and 2. Then, for each slit n, we compare the optical phase of the scattered field $E_{n,m}$ from that slit at the desired output position $\mathbf{r}_m^F$, and the phase of the total scattered field E_m^{total} (from all the slits) at the same position $\mathbf{r}_m^F$. We are interested in understanding to what extent the phase of $E_{n,m}$ is adding optimally constructively to E_m^{total}. The idea here is to deduce how we might adjust the position of this slit so that the phase of its scattering is such that this scattering contributes as strongly as possible to the resulting total field at the desired output position. For any given wavelength λ_m and corresponding output position $\mathbf{r}_m^F$, the phase difference could be formally expressed as $\arg(E_m^{\text{total}} E_{n,m}^* / [|E_m^{\text{total}}||E_{n,m}|])$. Of course, we need to choose that adjustment to the slit position so that it is a good compromise position that works well for all the desired operating wavelengths λ_m and corresponding output positions $\mathbf{r}_m^F$. So, we evaluate an overall phase mismatch factor δ_n that is effectively averaged over all the

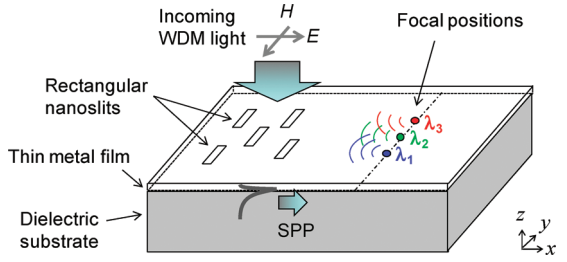

Figure 1. Schematic of multiple-wavelength focusing plasmonic coupler. When wavelength-multiplexed light shines on the nanoslit pattern, SPP waves are excited and propagate in the $x-y$ plane at the metal–dielectric interface. With proper design of the slit pattern, SPPs at different wavelengths are focused into different respective focal positions.

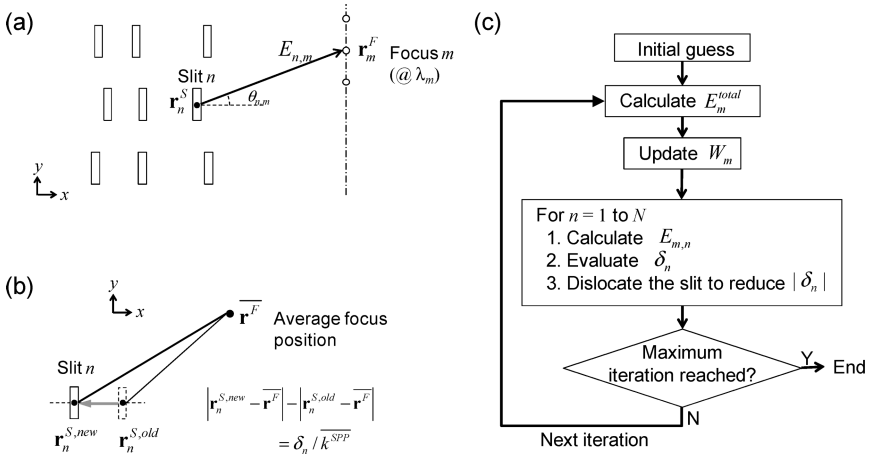

Figure 2. (a) Top view of the structure with the definitions of parameters used in the analysis. The total field at focus m is the sum of the contribution (defined as $E_{n,m}$) from each slit. (b) Geometrical explanation of dislocating the slit in each iteration step. The new location $\mathbf{r}_n^{s,\text{new}}$ is chosen to reduce the magnitude of the phase mismatch factor δ_n. (c) Flowchart of the optimization algorithm.

dx.doi.org/10.1021/nl200938h |Nano Lett. 2011, 11, 2693–2698

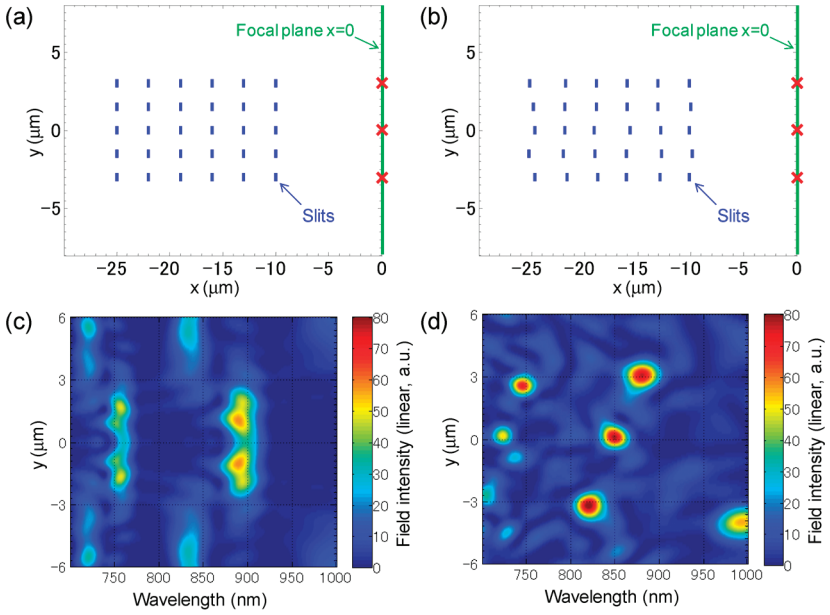

Figure 3. (a) Periodic slit pattern used as the initial guess and (b) the nonperiodic pattern obtained after 40 iteration steps. The three red crosses represent the locations chosen as the desired focal positions for the wavelengths, 820 (bottom), 850 (middle), and 880 (top) nm. (c) Field intensity at $x = 0$ as a function of position y (vertical axis) and wavelength (horizontal axis) for the periodic pattern shown in (a). (d) Same intensity map for the nonperiodic pattern shown in (b). As a result of the optimization process, three distinct spots emerge in (d), indicating that SPPs at wavelengths of 820, 850, and 880 nm are focused to points $(x, y) = (0, -3\ \mu\text{m})$, $(0, 0)$, and $(0, 3\ \mu\text{m})$, respectively.

desired operating wavelengths and positions defined by

$$\delta_n \equiv \arg\left[\sum_m W_m \frac{E_m^{\text{total}} E_{n,m}^*}{|E_m^{\text{total}}||E_{n,m}|}\right] \quad (3)$$

Here, we introduce the weight factor W_m to obtain a uniform intensity distribution among the M desired outputs in fewer iteration steps. W_m is initially defined to be 1 for all m and is updated in each iteration step according to the relation

$$W_m^{\text{new}} = W_m^{\text{old}} \left(\frac{\max(|E_m^{\text{total}}|^2)}{|E_m^{\text{total}}|^2}\right)^q \quad (4)$$

where max denotes the maximization over all the foci ($m = 1, ..., M$) and the factor q is chosen small enough to avoid instability of the algorithm.[17] Throughout this work, we use $q = 0.1$.

Using the phase mismatch factor δ_n obtained by eq 3, the position of slit n is then adjusted (dislocated) to reduce $|\delta_n|$. For simplicity, we only move the slit in the x direction. As illustrated in Figure 2b, the new position of the slit $\mathbf{r}_n^{\text{S,new}}$ is determined from the old position $\mathbf{r}_n^{\text{S,old}}$ to satisfy $|\mathbf{r}_n^{\text{S,new}} - \mathbf{r}^{\text{F}}| - |\mathbf{r}_n^{\text{S,old}} - \mathbf{r}^{\text{F}}| = \delta_n / k^{SPP}$, where $\mathbf{r}^{\text{F}} = \langle \mathbf{r}_m^{\text{F}} \rangle$ is the average position of all the foci and $k^{SPP} = \langle k_m^{\text{SPP}} \rangle$ is the propagation constant of the SPP wave averaged over all desired operating wavelengths λ_m. We iterate these steps until we obtain acceptable performance. Here, we are implicitly assuming that the small change in the phase of total field resulting from the movement of a single slit is approximately negligible in each iteration step. Such an assumption is reasonable for relatively weak scattering from each of a relatively large number of slits. We should also note that the accuracy of determining the next slit position in each step is not critical in obtaining an optimized structure. As long as we move the slit in the correct direction every time, the slit pattern converges to a similar design after sufficient number of iterations. Any other gradient-based optimization algorithm, such as the steepest-descent method should also be effective.

As an example, we design a triplexer (a three-wavelength multiplexer/demultiplexer) that focuses light at three wavelengths, 820, 850, and 880 nm, into different well-separated positions. Figure 3a illustrates a 6×5 periodic slit pattern, used as the initial guess in the optimization process. We assume an Au film with a thickness of 75 nm on a glass substrate and choose a slit dimension of 100 and 500 nm in the x and y directions, respectively. From 3D-FDTD simulation, we confirmed that with the slit length shorter than 600 nm in the y direction, the SPP radiation pattern at the 850 nm wavelength range is well approximated by a dipole radiation pattern. The three focusing points are set to $(x, y) = (0, -3\ \mu\text{m})$, $(0, 0)$, and $(0, 3\ \mu\text{m})$. The slits are located 10 μm away from the foci in the $-x$ direction, and adjacent slits are separated initially by 3 μm in the x and 1.5 μm in the y directions, making the total pattern size to be 15 μm $\times$ 6 μm. We assume an x-polarized Gaussian beam with a beam diameter ($1/e^2$ width) of 17 μm focused onto the center of the nanoslit pattern. Note that the initial slit pattern and focusing positions are chosen somewhat arbitrarily in this work for the proof-of-concept demonstration, but we ensured that the total pattern size is large enough to realize the required spectral resolution of the targeted characteristic.

Figure 3b shows the resultant slit pattern obtained after 40 iteration steps of optimization. It shows that the slits are dislocated in the x direction and that their spacings are no longer periodic. Figure 3c,d compares the spectra at the focal plane ($x = 0$) for the periodic (Figure 3a) and nonperiodic (Figure 3b) patterns, respectively. The vertical axis denotes the y position along the line $x = 0$, and the horizontal axis denotes the wavelength. For the case of the initial periodic structure (Figure 3c), the spectral feature is symmetric with respect to y, whereas for the nonperiodic structure (Figure 3d), three discrete

dx.doi.org/10.1021/nl200938h |*Nano Lett.* 2011, 11, 2693–2698

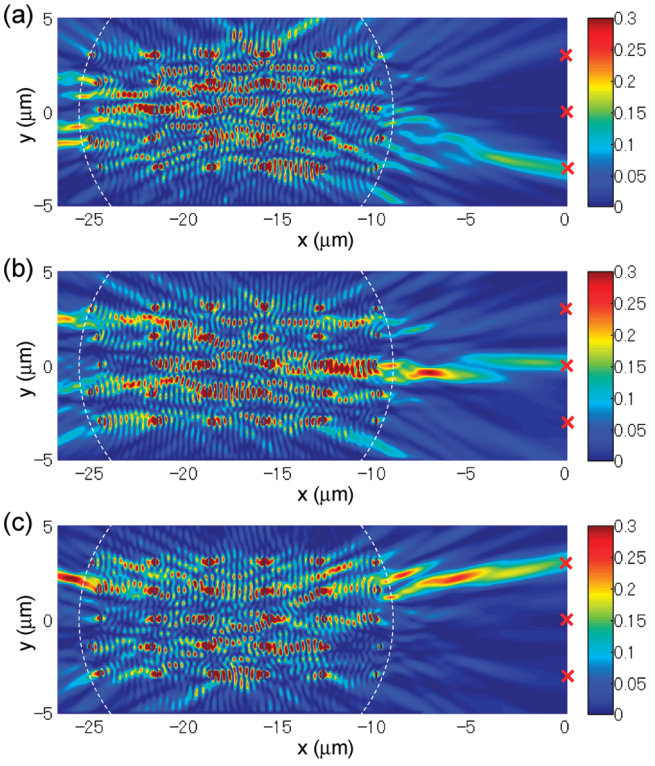

Figure 4. 3D-FDTD-simulated electric field intensity $|E_z|^2$ of the SPP wave at the *xy*-plane just beneath the Au film at three wavelengths: (a) 820 nm, (b) 850 nm, and (c) 880 nm. The slit pattern designed in Figure 3b is employed and an *x*-polarized Gaussian beam with 17 μm beam waist diameter is focused onto the center of the nanoslit pattern (as indicated by the white dashed circles). The intensity is normalized to the peak intensity $|E_x|^2$ of the input beam at the metal surface. In order to show the focusing features clearly, the intensity in the vicinity of slits is saturated in these false color plots. The red crosses indicate the predefined three focal positions used in the design. (A movie showing the field pattern for the entire spectral range from 800 to 900 nm is available in the Supporting Information.)

spots appear, indicating that SPPs at wavelengths of 820, 850, and 880 nm, respectively, are focused into different locations, $(x, y) = (0, -3\ \mu\text{m})$, $(0, 0)$, and $(0, 3\ \mu\text{m})$.

It is interesting to note that this demultiplexer has a qualitatively different behavior from conventional periodic grating devices, which would have continuous dispersion bands if we drew a similar *y*-wavelength map, corresponding to the output position changing smoothly with wavelength. Instead here we have engineered a device that puts one band of wavelengths substantially at one specific position, another at a second, and so on. From the point of view of applications, these well-separated discrete peaks in Figure 3d imply that spectral broadening or shifting would not occur even if the photodetecting element at the focus has a finite width or has some misalignment in *y*-direction. This behavior is similar to the stepped dispersion pattern designed in a previous nonperiodic layered dielectric stack structure.[14] This feature might be an important advantage to allow larger tolerance in fabrication and also illustrates the ability of such nonperiodic structures to generate desired responses not readily possible with simple periodic approaches.

The demultiplexing function of the nanoslit structure designed in Figure 3b is verified numerically by 3D FDTD simulation.[18] An *x*-polarized Gaussian beam with a 17 μm beam waist diameter is focused onto the center of the pattern and the SPP field at the *xy*-plane beneath the Au film is recorded after a sufficient time of propagation. To save computational effort, we perform FDTD simulation on a limited 3D volume of 20 μm × 10 μm × 2 μm surrounding the entire nanoslit pattern, and then interpolate the SPP field in the complete *xy*-plane analytically by the near-to-far-field transformation. Figure 4 shows the simulated electric field intensity $|E_z|^2$ of the SPP wave in the *xy*-plane just beneath the Au film at the three wavelengths of 820, 850, and 880 nm. A movie showing the field pattern for the entire spectral range from 800 to 900 nm is also available in the Supporting Information. The intensity is normalized to the peak intensity $|E_x|^2$ of the incident beam launched at the Au surface. The figures clearly display that the three wavelengths are sorted to their desired focal positions (indicated by the red crosses in the figures) specified in the design.

The designed plasmonic demultiplexer was fabricated to investigate the concept experimentally. Figure 5 shows the scanning electron microscope (SEM) image of the fabricated device (Figure 5a) with the magnified view of the slits (Figure 5b) and the schematic of the cross section (Figure 5c). The slits were 120 nm wide in the *x* direction and 520 nm long in the *y*-direction. At the focal position, a silicon metal−semiconductor−metal (MSM) photodiode was integrated to measure the photocurrent spectrum. The entire device was formed on a silicon-on-pyrex (SOP) platform, which was fabricated by anodically bonding an oxidized silicon-on-insulator (SOI) wafer to a glass (pyrex) substrate and then removing the handle silicon substrate.[19] The silicon device layer was first etched to form the photodetector mesa and a layer of Cr/Au/Cr was used to form contact pads with electron-beam evaporation and subsequent lift-off, forming back-to-back Schottky contacts to the silicon. A 75 nm thick film of Au was deposited directly on the glass surface, followed by a 5 nm thick Ti layer, both by electron-beam evaporation, and the overall region of this film was patterned using liftoff to form the metallic region for the demultiplexer region. The nanoslit array was defined in this Ti/Au film by electron-beam lithography and etched by Ar-ion sputtering. Note that the Au film sits directly on the pyrex glass so as to minimize any SPP propagation losses that could result from additional metal layers that might otherwise have been used to enhance adhesion. To examine multiple focusing at the individual focal positions, we prepared three different samples, Chip 1, Chip 2, and Chip 3, having the identical slit patterns but in which the slit pattern was offset in the *y*-direction by 3, 0, and −3 μm, respectively, so as to emulate one device with three detectors spaced by 3 μm from each other. We should note that the nanoslits would also excite SPPs at the upper Ti−air interface as well. Because of the deliberate presence of the Ti layer and its large propagation loss at 850 nm wavelength, however, the propagation length of this SPP mode is estimated to be as short as 1.2 μm, so that its effect is safely neglected.

An *x*-polarized wavelength-tunable Ti-Sapphire laser beam with a beam waist of 12 μm diameter was incident onto the slit structure at normal incidence and the photocurrent at the silicon MSM photodiode was recorded as a function of wavelength. Figure 6a shows the normalized photocurrent spectra measured for Chips 1, 2, and 3. Spectral peaks are observed at 822, 850, and 880 nm with 3-dB bandwidths of 16, 18, and 12 nm, respectively. We also plot in Figure 6b the calculated spectra for the three focal positions, which include the effects both of finite spectral line width of the laser light (5−9 nm in the measured wavelength

dx.doi.org/10.1021/nl200938h |*Nano Lett.* 2011, 11, 2693–2698

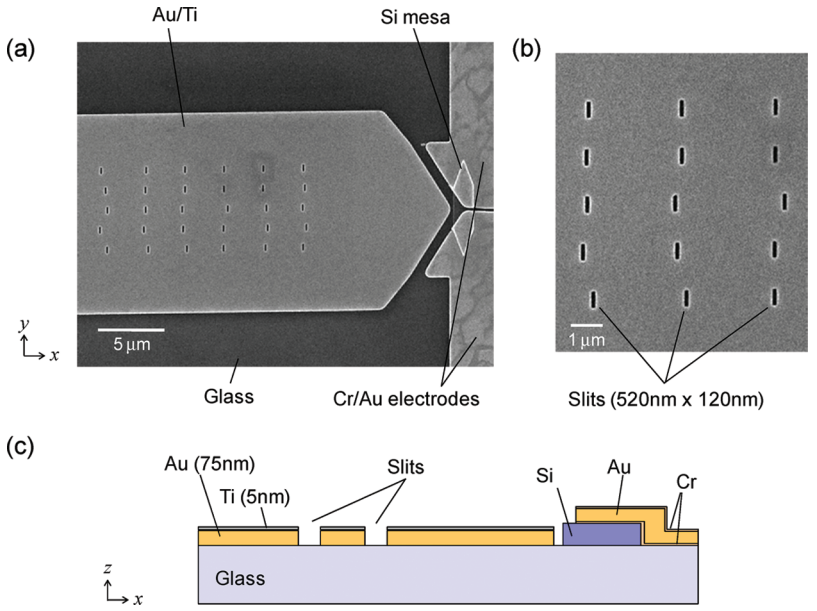

Figure 5. (a) SEM image of the fabricated device (Chip 2), (b) magnified image at the slits (showing the second, third and fourth columns of slits from left to right), and (c) the schematic of the cross section. The nonperiodic plasmonic grating coupler designed in Figure 3b is integrated with a silicon MSM photodetector. To test the multiple-wavelength focusing, three chips, Chip 1, Chip 2, and Chip 3, were fabricated with the slit pattern offset by 3, 0, and −3 μm in y-direction, respectively.

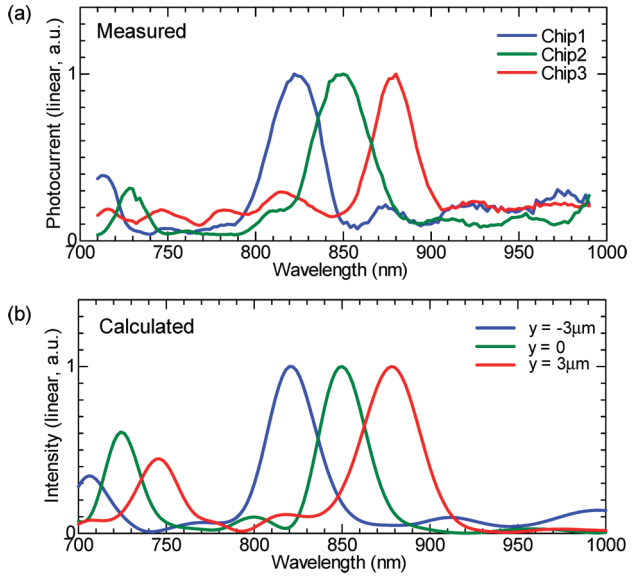

Figure 6. (a) Measured photocurrent spectra under normal illumination for the three devices, Chip 1, 2, and 3, which have the identical slit pattern, offset by 3, 0, and −3 μm in y-direction, respectively. (b) Calculated SPP intensity at the three focal positions $y = -3$, 0, and 3 μm ($x = 0$). Close agreement is observed between the measurement and calculation.

range since the source was actually a short-pulse mode-locked laser) and of the actual beam diameter (12 μm), which was narrower than that assumed in the design (17 μm). Close agreement between the measurement and calculation verifies the effectiveness of our rather simplified design scheme based on the Huygens−Fresnel principle.

Finally, we note that the proposed scheme should also be applicable in designing grooves to excite SPPs in the upper metal−air interface.[11,13] The SPP mode in the lower metal−dielectric interface demonstrated in this work, however, has an important advantage that it could be focused down laterally to subwavelength scales by simply tapering the width of metal strip,[20] whereas the upper air-guided SPP mode has a cutoff waveguide width.[21] One obvious application of our demultiplexer is that by applying nanofocusing tapers at the focal positions and integrating an array of nanometer-scale photodiodes, we could build a compact WDM receiver with ultralow-capacitance detectors.[22,23] Such a device is particularly attractive in constructing high-speed low-power optical interconnects, where WDM could play an important role of solving the strict requirements of wiring density.[24]

In conclusion, we have proposed and demonstrated both numerically and experimentally that a nonperiodic nanoslit array on a thin metal film can be used to couple free-space light to SPPs and simultaneously demultiplex different wavelengths into individual focal positions. A simple iterative optimization algorithm was used to tune the location of each nanoslit to obtain the desired SPP wavefront in the 2D plane of metal−dielectric interface. By measuring the photocurrent spectrum of the integrated silicon photodetector, we have experimentally demonstrated that SPPs at wavelengths of 820, 850, and 880 nm are sorted to three different focal positions, in close agreement with the design. One interesting feature of this demultiplexer is that the focal position hops discretely from one predefined position to the other as we sweep the wavelength. Such behavior is qualitatively different from that of conventional periodic grating devices, where the output position changes continuously with wavelength. These results illustrate the potential of such nonperiodic structures to generate complicated spectral responses that are not readily possible with simple periodic approaches. The proposed structure is directly applicable to the plasmonic nanofocusing waveguide demonstrated recently[20] and would provide a simple method of building a multiple-wavelength

dx.doi.org/10.1021/nl200938h |*Nano Lett.* 2011, 11, 2693–2698

nanometer-scale photodetector array for WDM optical interconnects, spectral imaging, and sensing applications.

■ ASSOCIATED CONTENT

Supporting Information. A movie showing the FDTD-simulated SPP field pattern for the entire spectral range from 800 to 900 nm is available. This material is available free of charge via the Internet at http://pubs.acs.org.

■ AUTHOR INFORMATION

Corresponding Author
*E-mail: tanemura@ee.t.u-tokyo.ac.jp.

■ ACKNOWLEDGMENT

The authors acknowledge the support of the IFC Focus Center, one of six research centers funded under the Focus Center Research Program, a Semiconductor Research Corporation program, and of the AFOSR Robust and Complex On-Chip Nanophotonics MURI. T.T. acknowledges the financial support from the Japan Society for the Promotion of Science (JSPS). K.C.B. acknowledge financial support from STMicroelectronics Stanford Graduate Fellowship. D.S.L.G. acknowledge financial support from Sequoia Capital Stanford Graduate Fellowship. P.W. acknowledges the Belgian American Education Foundation (BAEF). Work was performed in part at the Stanford Nanofabrication Facility (a member of the National Nanotechnology Infrastructure Network) that is supported by the National Science Foundation under Grant ECS-9731293, its lab members, and the industrial members of the Stanford Center for Integrated Systems. We are pleased also to acknowledge Elizabeth Edwards for developing the specific anodic bonding process we used here.

■ REFERENCES

(1) Barnes, W. L.; Dereux, A.; Ebbesen, T. W. Surface plasmon subwavelength optics. *Nature* **2003**, *424*, 824–830.

(2) Schuller, J. A.; Barnard, E. S.; Cai, W.; Jun, Y. C.; White, J. S.; Brongersma, M. L. Plasmonics for extreme light concentration and manipulation. *Nat. Mater.* **2010**, *9*, 193–204.

(3) Atwater, H. A.; Polman, A. Plasmonics for improved photovoltaic devices. *Nat. Mater.* **2010**, *9*, 205–213.

(4) Gramotnev, D. K.; Bozhevolnyi, S. I. Plasmonics beyond the diffraction limit. *Nat. Photonics* **2010**, *4*, 83–91.

(5) Lopez-Tejeira, F.; Rodrigo, S. G.; Martin-Moreno, L.; Garcia-Vidal, F. J.; Devaux, E.; Ebbesen, T. W.; Krenn, J. R.; Radko, I. P.; Bozhevolnyi, S. I.; Gonzalez, M. U.; Weeber, J. C.; Dereux, A. Efficient unidirectional nanoslit couplers for surface plasmons. *Nat. Photonics* **2007**, *3*, 324–328.

(6) Yin, L.; Vlasko-Vlasov, V. K.; Pearson, J.; Hiller, J. M.; Hua, J.; Welp, U.; Brown, D. E.; Kimball, C. W. Subwavelength focusing and guiding of surface plasmons. *Nano Lett.* **2005**, *5*, 1399–1402.

(7) Liu, Z.; Steele, J. M.; Srituravanich, W.; Pikus, Y.; Sun, C.; Zhang, X. Focusing surface plasmons with a plasmonic lens. *Nano Lett.* **2005**, *5*, 1726–1729.

(8) Steele, J. M.; Liu, Z.; Wang, Y.; Zhang, X. Resonant and non-resonant generation and focusing of surface plasmons with circular gratings. *Opt. Express* **2006**, *14*, 5664–5670.

(9) Ditlbacher, H.; Krenn, J. R.; Schider, G.; Leitner, A.; Aussenegg, F. R. Two-dimensional optics with surface plasmon polaritons. *Appl. Phys. Lett.* **2002**, *81*, 1762–1764.

(10) Nomura, W.; Ohtsu, M.; Yatsui, T. Nanodot coupler with a surface plasmon polariton condenser for optical far/near-field conversion. *Appl. Phys. Lett.* **2005**, *86*, 181108.

(11) Laux, E.; Genet, C.; Skauli, T.; Ebbesen, T. W. Plasmonic photon sorters for spectral and polarimetric imaging. *Nat. Photonics* **2008**, *2*, 161–164.

(12) Drezet, A.; Koller, D.; Hohenau, A.; Leitner, A.; Aussenegg, F. R.; Krenn, J. R. Plasmonic crystal demultiplexer and multiports. *Nano Lett.* **2007**, *7*, 1697–1700.

(13) Zhao, C.; Zhang, J. Plasmonic demultiplexer and guiding. *ACS Nano* **2010**, *4*, 6433–6438.

(14) Gerken, M.; Miller, D. A. B. Multilayer thin-film stacks with steplike spatial beam shifting. *J. Lightwave Technol.* **2004**, *22*, 612–618.

(15) Zhao, C.; Zhang, J. Binary plasmonics: launching surface plasmon polaritons to a desired pattern. *Opt. Lett.* **2009**, *34*, 2417–2419.

(16) Chang, S. H.; Gray, S. K.; Schatz, G. C. Surface plasmon generation and light transmission by isolated nanoholes and arrays of nanoholes in thin metal films. *Opt. Express* **2005**, *13*, 3150–3165.

(17) Backlund, J.; Bengtsson, J.; Carlstrom, C. F.; Larsson, A. Incoupling waveguide holograms for simultaneous focusing into multiple arbitrary positions. *Appl. Opt.* **1999**, *38*, 5738–5746.

(18) Wahl, P. D. S.; Ly-Gagnon, Debaes, C.; Miller, D. A. B.; Thienpont, H. *Open-source GPU-based 3D-FDTD with multi-pole dispersion for plasmonics*, 11th International Conference on Numerical Simulation of Optoelectronic Devices (NUSOD), 5−8 September, 2011, Rome, Italy; Paper MB2.

(19) Ly-Gagnon, D. S.; Balram, K. C.; White, J. S.; Wahl, P.; Brongersma, M. L.; Miller, D. A. B. *On-chip optical propagation and photodetection in nanometer-scale two-conductor plasmonic waveguides*, 3rd Int. Top. Meeting on Nanophotonics and Metamaterials, 3−6 January, 2011, Seefeld, Tirol, Austria; Paper TUE4f.64.

(20) Verhagen, E.; Spasenovic, M.; Polman, A.; Kuipers, L. Nanowire plasmon excitation by adiabatic mode transformation. *Phys. Rev. Lett.* **2009**, *102*, 203904.

(21) Zia, R.; Schuller, J. A.; Brongersma, M. L. Near-field characterization of guided polariton propagation and cutoff in surface plasmon waveguides. *Phys. Rev. B* **2006**, *74*, 165415.

(22) Ishi, T.; Fujikata, J.; Makita, K.; Baba, T.; Ohashi, K. Si nano-photodiode with a surface plasmon antenna. *Jpn. J. Appl. Phys.* **2005**, *44*, L364–L366.

(23) Tang, L.; Kocabas, S. E.; Latif, S.; Okyay, A. K.; Ly-Gagnon, D. S.; Saraswat, K. C.; Miller, D. A. B. Nanometre-scale germanium photodetector enhanced by a near-infrared dipole antenna. *Nat. Photonics* **2008**, *2*, 226–229.

(24) Miller, D. A. B. Device requirements for optical interconnects to silicon chips. *Proc. IEEE* **2009**, *97*, 1166–1185.